# Magnetic and electronic properties of the ferromagnetic Kondo-lattice system $Np_2PdGa_3$

V. H. Tran,[1] J.-C. Griveau,[2] R. Eloirdi,[2] W. Miiller,[1] and E. Colineau[2]
[1]*Institute of Low Temperature and Structure Research, Polish Academy of Sciences, P.O. Box 1410, 50-950 Wrocław, Poland*
[2]*Joint Research Centre, Institute for Transuranium Elements, European Commission, Postfach 2340, D-76125 Karlsruhe, Germany*
(Received 25 May 2010; published 3 September 2010)

Intermetallic compounds $Lu_2PdGa_3$ and $Np_2PdGa_3$ have been found to crystallize in an orthorhombic $CeCu_2$-type structure with the *Imma* space group. The lattice parameters at room temperature are: $a=0.4382(2)$, $b=0.6870(3)$, and $c=0.7593(3)$ nm for $Lu_2PdGa_3$ and $a=0.4445(2)$, $b=0.7089(3)$, and $c=0.7691(3)$ nm for $Np_2PdGa_3$. The electronic ground-state properties of these compounds were established by magnetic, calorimetric, electrical resistivity, magnetoresistance, and Hall coefficient measurements. The experimental data reveal a metallic behavior for Pauli paramagnetic $Lu_2PdGa_3$, characterized by Sommerfeld ratio $\gamma=2.5$ mJ/K$^2$ mol Lu and temperature-independent susceptibility $\chi_0 \sim 1\times10^{-4}$ emu/mol. In contrast to the nonmagnetic $Lu_2PdGa_3$ reference, $Np_2PdGa_3$ behaves as a local-moment ferromagnet with the Curie temperature $T_C=62.5(2)$ K. Low-temperature properties of $Np_2PdGa_3$ are characterized by a large Sommerfeld ratio $\gamma=120(2)$ mJ/K$^2$ mol Np and a small Fermi momentum $k_F=0.44$ Å$^{-1}$. The observed features in $Np_2PdGa_3$ are well interpreted by assuming competition of three different interactions: Rudermann-Kittel-Kasuya-Yosida (RKKY), crystal electric field (CEF) and Kondo effect, which are represented by respective energies $k_BT_{RKKY}$, $\Delta_{CEF}$, and $k_BT_K$. We argue that $Np_2PdGa_3$ is the Np-based ferromagnetic Kondo-lattice system with $T_K < T_{RKKY} \approx \Delta_{CEF}$.

DOI: 10.1103/PhysRevB.82.094407 PACS number(s): 71.27.+a, 75.30.−m, 75.20.Hr

## I. INTRODUCTION

A number of intermetallics of the stoichiometric compounds $U_2TM_3$, where $T=3d$, $4d$, and $5d$ electron transition metals and $M=$Si or Ga have been discovered.[1–3] Generally, these compounds adopt two well-known types of crystal structure, i.e., the hexagonal $AlB_2$- or orthorhombic $CeCu_2$-type, respectively. Most of the compounds which crystallize in the hexagonal $AlB_2$-type are those containing $M=$Si and showing spin-glass or ferromagnetic cluster glass behavior.[4–6] On the other hand, the compounds with $M=$Ga favor the $CeCu_2$-type and exhibit various types of magnetic ordering including spin fluctuation, ferromagnetic, and antiferromagnetic order at low temperatures.[3] Among $U_2TGa_3$, the magnetism of the Pd- and Pt-based compounds appears to be an enormously complex subject owing to an interplay of the Kondo effect and randomness for long-range antiferromagnetism.[7] The Kondo effect manifests itself in the electrical resistivity, magnetoresistance, and the enhancement of the electronic coefficient of the specific heat.[7] The latter behavior, in principle, indicates a strong correlation between $5f$ and conduction electrons at low temperatures. However, Gschneidner *et al.*,[8] pointed out that large electronic heat capacities may also arise from nonmagnetic atom disorder (NMAD) in compounds where $f$-electron atoms occupy a periodic lattice position. Actually, effect of crystal disorder in the $U_2PdGa_3$ compound is rather enormous, at least it contributes to a short-range magnetic order[7] and to nonzero spin chirality in the anomalous Hall coefficient.[9] In order to find out a comprehensive explanation or quantitative concept to understand the complex properties of $U_2TGa_3$ one should find answers to such questions such as: is the moment on $f$-electron ions localized or itinerant? What is the role of atomic disorder in determining physical properties? And what is the role of the hybridization between the $f$-electron and the transition metal ions involved in a given compound? Within the framework of these problems we are convinced that any investigation of a new system being isostoichiometic and/or isostructural to $U_2PdGa_3$ would be useful. Such series of intermetallic actinoid ($An$) compounds such as $(U,Np,Pu)_2TGa_3$ would provide an opportunity of a systematic study and thus might help us to answer the above given questions.

In this paper, we present the synthesis and crystallographic characterization, as well as the measurements of specific heat, magnetization, electrical resistivity, magnetoresistance and Hall effect for $Np_2PdGa_3$. The experimental data revealed that the ferromagnetic transition in $Np_2PdGa_3$ at 62.5 K is due to an exchange interaction between the localized magnetic $Np^{3+}$ moments via conduction electrons. We argue that at lower temperatures, the Kondo effect is responsible for the large values of the electronic specific-heat coefficient of ~120 mJ/K$^2$ mol Np. The large carrier effective mass (~170 $m_0$) estimated from the Hall coefficient and the specific heat at 2 K may classify the compound to the class of heavy-fermion materials. The obtained data for $Np_2PdGa_3$ are compared to those of the nonmagnetic reference $Lu_2PdGa_3$ and antiferromagnetic counterpart $U_2PdGa_3$, and are discussed in terms of three competing interactions: Rudermann-Kittel-Kasuya-Yosida (RKKY), crystal electric field (CEF), and Kondo effect, which are characterized by respective energies $k_BT_{RKKY}$, $\Delta_{CEF}$, and $k_BT_K$. Our results suggest that $Np_2PdGa_3$ is a Np-based ferromagnetic Kondo-lattice system with $T_K < T_{RKKY} \approx \Delta_{CEF}$. It seems that for the magnetic behavior of $Np_2PdGa_3$ can be understood on the basic of an underscreened Kondo-lattice (UKL) model, recently developed by Perkins *et al.*[10] Among Np-based compounds, a similar ferromagnetic Kondo behavior was previously reported for $NpNiSi_2$.[11]

 

## II. EXPERIMENTAL DETAILS

Polycrystalline samples of $Lu_2PdGa_3$ and $Np_2PdGa_3$ (0.5 g) were synthesized from high-purity elements (Np 3N, Lu 4N, Pd 4N, and Ga 6N) by arc-melting under Ti-gettered argon purified atmosphere. To improve homogeneity the samples were turned over and remelted several times, then wrapped in tantalum and annealed in sealed quartz ampule for two weeks at 800 °C. After homogenization, the samples were characterized by standard x-ray powder diffraction and energy dispersive x-ray analysis.

Specific-heat measurements have been performed on $Lu_2PdGa_3$ and $Np_2PdGa_3$ using a thermal relaxation method in the temperature range 2–300 K and in external magnetic fields up to $B=\mu_0 H=9$ T, utilizing a commercial physical properties measurement system (Quantum Design-PPMS).

Measurements of magnetization $M$ were performed in the temperature range 2–300 K and in magnetic fields up to $\mu_0 H=7$ T using a superconducting quantum interference device magnetometer (Quantum Design—MPMS). The measurements were performed on the $Np_2PdGa_3$ sample in the field-cooled (FC) and zero-field-cooled (ZFC) modes.

The electrical resistivity $\rho(T)$ of $Lu_2PdGa_3$ and $Np_2PdGa_3$ was measured from 2 to 300 K by a conventional four-probe dc method using a PPMS (Quantum Design) with a current strength of $j=5$ mA. The magnetoresistance data were collected in magnetic fields up to 14 T, applied perpendicular to the current direction.

The Hall voltage $V_H(B)$ of $Np_2PdGa_3$ was measured between the transverse contacts in magnetic fields up to 9 T, perpendicular to the sample surface according to

$$V_H(B) = \frac{1}{2}[V(B) - V(-B)] \tag{1}$$

and the Hall coefficient was calculated from

$$R_H(B,T) = \frac{V_H(B,T)t}{Bj}, \tag{2}$$

where $t=112$ $\mu$m is the thickness of the sample. The $Np_2PdGa_3$ samples were encapsulated in specially designed sample holders. The response of the holder for magnetization and specific heat was measured separately before inserting the sample and then subtracted from measured raw data.

## III. EXPERIMENTAL DATA AND ANALYSIS

### A. Sample characterization

The x-ray diffraction data collected in the range $20° \leq 2\Theta \leq 100°$ for $Np_2PdGa_3$ are shown in Fig. 1. The patterns revealed that the majority phase (>95% of the mass) has the orthorhombic $CeCu_2$-type structure. We were able to identify $NpO_2$, "$Np_3Pd_3Ga_8$" and NpC as the main impurities. The literature describes $NpO_2$ with a cubic structure (space group $FM\bar{3}m$) to undergo into an electric quadrupole state below $T_0=25$ K (Ref. 12) while the cubic NpC (space group $FM\bar{3}m$) is antiferromagnetic between 310 and 220K, and ferromagnetic below 220 K.[13] One impurity phase is assigned as $Np_3Pd_3Ga_8$ because it is isostructural to $Lu_3Rh_3Ga_8$.[14]

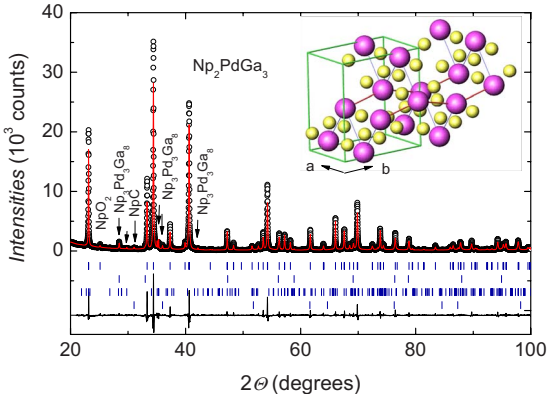


FIG. 1. (Color online) X-ray powder-diffraction pattern of $Np_2PdGa_3$. The observed (open circles), calculated (solid line) and the difference between observed and calculated data (bottom). The vertical bars indicate the positions of Bragg reflections for $Np_2PdGa_3$, $NpO_2$, $Np_3Pd_3Ga_8$, and NpC, respectively, from the top. Inset: crystal structure of $Np_2PdGa_3$. Large balls represent the Np atoms and small ones the Pd or Ga atoms. Note that the nearest Np neighbors form zigzag chains parallel to the $b$ axis (thick line) and the next-nearest Np neighbors are connected by zigzag chains along the a axis (thin line).

Crystal structure refinement based on the x-ray data indicated that $Np_3Pd_3Ga_8$ is orthorhombic with space group *Imma* and lattice parameters $a=0.42888(3)$, $b=0.95693(2)$, and $c=1.26061(5)$ nm. No information is available about magnetic properties of $Np_3Pd_3Ga_8$. Traces of these impurities are denoted by arrows in the diffraction pattern. We emphasize that influence of the impurities on magnetic behavior of $Np_2PdGa_3$ is not observed by the bulk properties measurements used in this work. It is likely that $Np_3Pd_3Ga_8$ is a paramagnet and does not make any significant contribution compared to the intrinsic contribution of $Np_2PdGa_3$, thus it is hard to detect by the measurements.

Refinement of the crystal structure of $Np_2PdGa_3$ based on 63 observed Bragg reflections was done with the Rietveld method using the Fullprof program.[15] The observed Bragg reflections for $Np_2PdGa_3$ were fitted with a pseudo-Voigt function profile. The final refinement converged at R-factor =1.1 and RF-factor=0.8. The observed Bragg reflections for $Np_2PdGa_3$ could be indexed with lattice parameters $a=0.4445(2)$ nm, $b=0.7089(3)$ nm, and $c=0.7691(3)$ nm. The Np atoms are located at the 4*e* (0, 1/4, $z_{Np}$) sites and the Pd and Ga atoms are distributed at the 8*h* (0, $y_{Pd/Ga}$, $z_{Pd/Ga}$) positions. The inset of Fig. 1 shows the crystal structure of $Np_2PdGa_3$ obtained for atomic position parameters equal to those refined for $U_2PdGa_3$ ($y_{Pd/Ga}=0.0385$, $z_{Pd/Ga}=0.1663$, and $z_U=0.5346$).[7] The nearest Np neighbors with the interatomic distance of $d1_{Np\text{-}Np}\sim 0.364$ nm, form the zigzag along the $b$ axis. The next (N)-nearest Np neighbors with $d2_{Np\text{-}Np}\sim 0.375$ nm form also zigzag chains but parallel to the $a$ axis. It may now be useful to compare the crystallographic data of $Np_2PdGa_3$ to those of $U_2PdGa_3$. A compilation of the lattice parameters and shortest interatomic distances for both compounds is given in Table I. Clearly, the substitution of neptunium for uranium causes an increase in the $a$ and $b$ parameters but practically no change in the $c$

TABLE I. Lattice parameters and nearest interatomic distances in $U_2PdGa_3$ and $Np_2PdGa_3$.

| Compounds | $U_2PdGa_3$ | $Np_2PdGa_3$ |
|---|---|---|
| $a$ (nm) | 0.4372 | 0.4445(2) |
| $b$ (nm) | 0.7017 | 0.7089(3) |
| $c$ (nm) | 0.7691 | 0.7691(3) |
| $d1_{An\text{-}An}$ (nm) | 0.360 | 0.364 |
| $d2_{An\text{-}An}$ (nm) | 0.373 | 0.375 |
| $d_{L\text{-}L}$ | 0.254 | 0.257 |
| $d_{An\text{-}L}$ | 0.172 | 0.173 |

parameter. Because the nearest Np neighbors are situated parallel to the $a$ and to the $b$ direction, the $a$ and $b$ parameters are naturally controlled by the size of $An$ ions. Taking into account the size of $An^{3+}$ and $An^{4+}$ ions,[16] one suspects that the increase in the lattice parameters is due to the substitution of the $U^{4+}$ ions with the ionic radius of 0.0918 nm by larger $Np^{3+}$ ions having the radius of 0.1017 nm. In $Np_2PdGa_3$ the shortest interatomic distance between ligands atoms $d_{L\text{-}L}$ is 0.257 nm, it is also larger than that in $U_2PdGa_3$. Interestingly, the distances between heteronuclear atoms are short ($d_{An\text{-}L}\sim 0.173$ nm) and approximately correspond to the sum of their ionic radii.

The x-ray diffraction data of $Lu_2PdGa_3$ allowed to conclude that this compound is isostructral to $Np_2PdGa_3$, possessing an orthorhombic $CeCu_2$-type structure. The lattice parameters of $Lu_2PdGa_3$ at room temperature are $a=0.4382(2)$, $b=0.6870(3)$, and $c=0.7593(3)$ nm.

### B. Specific heat

The specific-heat data of $Lu_2PdGa_3$ and $Np_2PdGa_3$ in the form $C_p(T)/T$ vs $T$, are presented in Fig. 2. For the specific heat of $Lu_2PdGa_3$ a good description is obtained with a relation: $C_p(T)=C_{el}+C_{ph}$, where the electronic contribution, $C_{el}$ is assumed to be $C_{el}=\gamma T$ and the lattice contribution $C_{ph}$ is represented by the sum of Debye and Einstein functions,[17]

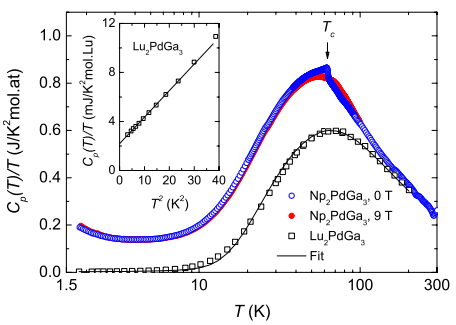


FIG. 2. (Color online) The specific heat of $Lu_2PdGa_3$ (squares) and $Np_2PdGa_3$ at 0 T (open circles) and at 9 T (closed circles) divided by temperature as a function of temperature. The line shows the fit to the sum of an electronic and a phonon term. Inset: low-temperature data of $Lu_2PdGa_3$ showing linear dependence of $C_p/T$ vs $T^2$.

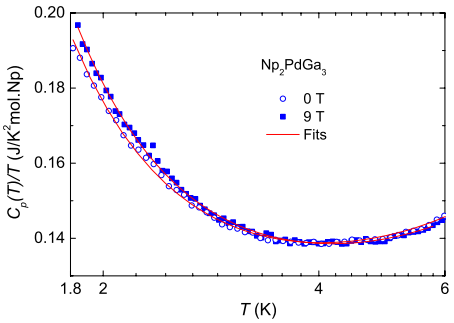


FIG. 3. (Color online) Low-temperature data of $Np_2PdGa_3$ showing splitting of the nuclear ground-state levels by hyperfine field of 230(3) T at 0 and 240(5) T at 9 T.

$$C_{ph}(T)=9Rn_D(T/\Theta_D)^3\int_0^{\Theta_D/T}\frac{x^4\,exp(x)}{[exp(x)-1]^2}dx + \frac{3Rn_E(\Theta_E/T)^2exp(\Theta_E/T)}{[exp(\Theta_E)-1]^2}, \quad (3)$$

where $R$ is the gas constant and $n_{D,E}$ is the number of Debye and Einstein vibrators and $\Theta_{D,E}$ are the Debye and Einstein temperature. The fit of the experimental data yielded $n_D=2$, $\Theta_D=315(5)$ K, $n_E=1$, and $\Theta_E=113(2)$ K. The coefficient of the electronic specific heat $\gamma=2.3(2)$ mJ/K$^2$ mol Lu can be evaluated by plotting $C_p/T$ vs $T^2$ shown in the inset of Fig. 2.

The specific heat of $Np_2PdGa_3$ achieves a value of 75 J/Kmol.Np at room temperature. Within experimental error limit this value match very well the Dulong-Petit value (74.8 J/Kmol.Np). The temperature dependence of $C_p(T)/T$ of $Np_2PdGa_3$ shows several remarkable features. First, an anomaly is observed at 62.4 K indicative of a magnetic phase transition due to the magnetic ordering of the $Np^{3+}$ ions. As revealed by magnetic measurements (see below), the nature of this transition is ferromagnetic. An application of a large magnetic field of 9 T completely smears out the magnetic phase transition, consistent with a ferromagnetic ordering. Second, a large $C_p/T$ ratio occurs at low temperatures, signifying the presence of strong correlated $5f$ electrons. Third, below 4 K there is clear upturn in $C_p/T$. This behavior can be attributed to the splitting of the nuclear ground-state level of the $^{237}$Np nuclei. The $^{237}$Np isotope with the nuclear moment $\mu_I=3.14$ $\mu_N$, may have six nuclear energy levels ranging from $I=-5/2$ to 5/2. In a simple two-level system, the hyperfine interaction characterized by the effective magnetic field $B_{hf}$ gives rise to a nuclear specific heat $C_N$ identifying with the Schottky specific heat $C_{Sch}$,[17]

$$C_{Sch}=R\left(\frac{\varepsilon}{k_BT}\right)^2\frac{g_0}{g_1}\frac{exp(\varepsilon/k_BT)}{\left[1+\frac{g_0}{g_1}exp(\varepsilon/k_BT)\right]^2}, \quad (4)$$

where $\varepsilon/k_B$ is the energy separation, $g_0$ and $g_1$ are the degeneracies of the two levels. The low-temperature specific-heat data of $Np_2PdGa_3$ are shown in Fig. 3. In fitting the data with the equation $C_p(T)/T=\gamma_{LT}+\beta T^2+C_N(T)/T$, we took into account the fit parameters $\gamma_{LT}$, $\beta$ and $\varepsilon/k_B$, and fixed the degeneracy ratio $g_0/g_1$ to be constant. It turns out that the

results of such a fit are not very sensitive to the magnitude of $g_0/g_1$ in the range 0.25 (singlet-quartet)–4 (quartet-singlet). Assuming an arbitrary ratio $g_0/g_1=1$, we obtain $\gamma_{LT}=123(1)$ mJ/K$^2$ mol Np, $\beta=0.57(2)$ mJ/K$^4$ mol Np and $\varepsilon/k_B=0.44(2)$ K. Based on the relation $B_{hf}=3\varepsilon k_B/(R^{0.5}\mu_I\mu_N)$ we obtain $B_{hf}=230(3)$ T, which corresponds to an ordered magnetic moment $M_{ord}=1.1\ \mu_B$ if assuming the relationship between the hyperfine field and the ordered magnetic moment 1 $\mu_B=215$ T.[18] The observed $B_{hf}$ value for $Np_2PdGa_3$ is smaller than those given for cubic $NpAl_2$ (316 T) and NpC (480 T),[19] or hexagonal $NpGa_2$ (525 T),[20] but higher than those in tetragonal $NpFeGa_5$ (203 T),[21] $NpCoGa_5$ (180 T),[22] and $NpRhGa_5$,(206 T) (Ref. 23) compounds. The applied magnetic field increases $B_{hf}$, which is found to slightly increase up to 240(5) T, i.e., about 6.5% at 9 T. We have failed to find any significant influence of the magnetic field on $\gamma_{LT}$, for instance, at a field of 9 T, $\gamma_{LT}$ persists practically at the same value as at 0 T. One tries to explain the effect of magnetic fields on the electronic specific heat using the resonance level model developed by Schotte and co-workers.[24,25] According to the model, the Kondo resonance is given by a Lorentzian

$$N(E_F)=\frac{\pi k_B^2 N_A}{3}\frac{\Gamma}{\Gamma^2+E^2}, \tag{5}$$

where $E$ is the Zeeman energy of the magnetic moment and $\Gamma$ is the width of the Kondo-resonance peak and it takes the magnitude on the order of the Kondo temperature $\sim k_B T_K$. Since the Kondo resonance varies with magnetic field strength as $\Gamma^2=\Gamma_0^2+(g\mu_B H)^2$ and $E=g\mu_B H$, the application of magnetic fields should decrease the density of states $N(E_F)$. The lack of a clear field dependence of the electronic specific heat implies that in an energy scale the width $\Gamma_0$ (i.e., $\sim k_B T_K$) is considerably larger than the applied field strength.

The contribution of 5$f$ electrons to the total specific heat, $C_{5f}=C_p-(C_{ph}+C_N)$, is obtained by subtracting the lattice part using the phonon contribution of the reference compound $Lu_2PdGa_3$ and the nuclear part considered above. As shown in Fig. 4(a), the $C_{5f}(T)/T$ vs $T$ curve shows a broad maximum at around 25 K, which suggests the CEF splitting of energy levels of the $Np^{3+}$ ions. Preliminary estimation of CEF levels evokes that the degeneracies of the two low-lying levels should have the ratio $g_0/g_1=2/3$ or 1, corresponding to one of four possible schemes: doublet-triplet or singlet-singlet, doublet-doublet, and triplet-triplet.

Normally in the orthorhombic symmetry ($D_{2h}$), the $J=4$ state of the $^5I_4$ multiplet for $Np^{3+}$ should be split into nine distinct, nondegenerate energy levels. However, the observed magnetic phase transition at 62.4 K indicates a magnetic ground state, thus ruling out the existence of any ground state singlet in this compound. Alternatively, the orthorhombic $CeCu_2$-type structure is very close related to the $AlB_2$-type structure (space group $P6/mmm$) and it is easily transformed from one into another, according to a relation $a_{ort}=a_{hex}$, $b_{ort}=2c_{hex}$, and $c_{ort}=a_{hex}\sqrt{3}$. In the hexagonal notation, the atomic parameters are a little shifted from the Wyckoff positions for the space group $P6/mmm$, i.e., for the

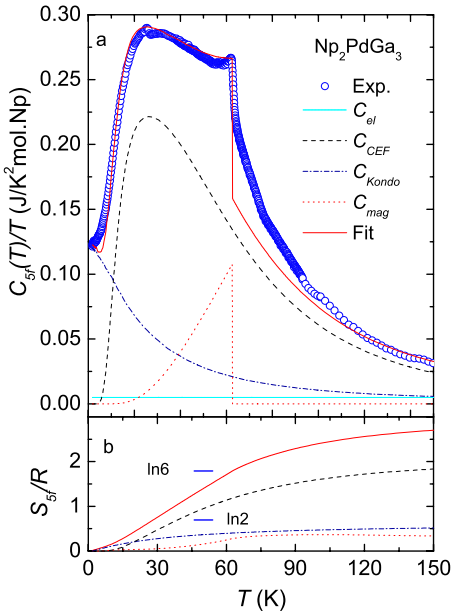


FIG. 4. (Color online) (a) Comparison of 5$f$-electron specific heat of $Np_2PdGa_3$ with calculated CEF, Kondo and magnon contributions to $C_p$. (b) 5$f$- electron entropy as a function of temperature. Symbols denote same meanings as in the upper panel.

Np atoms the shift is $(z_{Np}-0.5)\sim 0.03$, for Pd and Ga by $(y_{Pd/Ga}-0)\sim 0.04$ and $(z_{Pd/Ga}-1/6)\sim 0.001$. In a quasihexagonal symmetry ($D_{6h}$), the $J=4$ state may split into three magnetic doublets ($2\Gamma_5,\Gamma_6$) and three singlets ($\Gamma_1,\Gamma_3$ and $\Gamma_4$). Two CEF level schemes, namely, doublet-doublet-singlet and doublet-doublet-doublet were tested by fitting the data. The fits clearly reveal that an assumption of the presence of a singlet leads to lower CEF contribution to the specific heat below $T_C$ and failing of fitting the magnetic specific heat, $C_{mag}$, i.e., resulting broad maximum below $T_C$ could not be explained from a change in the specific heat by magnon scattering. It turns out a doublet-doublet-doublet configuration with an energy splitting of $\Delta_1=60$ and $\Delta_2=180$ K is most consistent with the data. These doublets have the ground state eigenfunctions as follows:

$$\Gamma_5^1=a|\pm 4\rangle+b|\mp 2\rangle, \tag{6}$$

$$\Gamma_5^2=b|\pm 4\rangle-a|\mp 2\rangle, \tag{7}$$

$$\Gamma_6=|\pm 1\rangle, \tag{8}$$

where $a=0.998$ and $b=0.063$. The specific heat due to the splitting of such a CEF scheme is illustrated as dashed line in Fig. 4(a). We should stress that the scenario assuming triplet-triplet and doublet-triplet ground state is hardly probable since it requires a cubic symmetry of the $Np^{3+}$, being significantly different from the present orthorhombic symmetry.

As clearly seen in Fig. 4(a), the $C_{5f}(T)/T$ ratio has a large value of $\sim 120$ mJ/K$^2$ mol Np at 2 K, being huge compared to those observed in 5$f$-electron ferromagnetic Kondo-lattice systems, such as $NpNiSi_2$ (65 mJ/K$^2$ mol Np),[11] and $UCo_{0.5}Sb_2$ (35.6 mJ/K$^2$ mol U).[26] The effects of spin-glass ordering or NMAD can be neglected in the compound stud-

ied here. For $Np_2PdGa_3$, $C_{5f}(T)/T$ at low temperatures practically does not change with applied fields up to 9 T. This behavior is completely different from the one observed for classical spin-glass $Eu_{1-x}Sr_x$ alloys,[27] where the Sommerfeld ratio was found to be very sensitive to applied magnetic fields. Furthermore, we do not find $C_{5f} \propto T^2$ dependence, which might characterize spin-glasslike behavior.[28] Therefore, presumably neither spin-glass nor NMAD effect are suitable mechanism for the enhancement in the electronic specific heat of $Np_2PdGa_3$. In order to verify spin-glasslike mechanism, eventual ac-magnetic susceptibility measurements on $Np_2PdGa_3$ would have been interesting.

We believe that the enhancement in the $C_{5f}(T)/T$ ratio of $Np_2PdGa_3$ at low temperatures is due to the Kondo effect. A strong support for this argument arises from comparison of the 5*f*-electron specific heat with Kondo contribution $C_{Kondo}$ inferred from the solution of the Coqblin-Schrieffer (CS) model for $J=1/2$ by Rajan.[29,30] In the CS model, the characteristic temperature $T_K$, which accounts for the energy scale of the Kondo interaction, is given by a relation: $T_K \sim \pi R/(6\gamma)$. Taking $\gamma=120$ mJ/K$^2$ mol Np we derive $T_K=36$ K and the Kondo contribution $C_{Kondo}$ to $C_{5f}$ is shown as dashed-dotted line in Fig. 4(a). Another estimation of the Kondo temperature comes from an approach of Bredl *et al.*[25] within a mean-field theory. As shown by Blanco *et al.*[31] $T_K$ and $T_C$ are related via the formula

$$\Delta C = \frac{6k_B}{\Psi'''\left(\frac{1}{2}+\zeta\right)}\left[\Psi'\left(\frac{1}{2}+\zeta\right)+\zeta\Psi''\left(\frac{1}{2}+\zeta\right)\right]^2, \quad (9)$$

where $\zeta=\frac{T_K}{2\pi T_C}$ and $\Psi'$, $\Psi''$, and $\Psi'''$ are the first three derivatives of the digamma function. Using Eq. (9) for $\Delta C(62.4K)=C_{5f}-C_{\mathrm{CEF}}=7.67$ J/K mol Np and $T_C=62.4$ K we obtain $T_K=32$ K. This value is close to $T_K$ deduced from the CS model considered above. The observation of a large $T_K$ would corroborate the weak field dependence of the electronic specific-heat coefficient, discussed above.

In common ferromagnets below $T_C$, magnons contribute to the total specific heat. The corresponding contribution $C_{mag}$ is given by $C_{mag}=C\times T^{3/2}$, where $C$ is a constant. Due to the orthorhombic crystal structure of the studied compound, the magnetocrystalline anisotropy may lead to the appearance of anisotropy gap $\Delta$ in the spin-wave spectrum. In this case, the magnon specific heat can be written as,[28]

$$C_{mag} = C \times T^{3/2}\, exp(-\Delta/k_B T). \quad (10)$$

The agreement between the measured $C_{5f}$ and calculated specific heat assuming $C_{5f}=C_{el}+C_{\mathrm{CEF}}+C_{Kondo}+C_{mag}$ for $T<T_C$ is rather good, if one can adjust parameter $C$ and $\Delta/k_B$ in Eq. (10) to 0.053 J/K$^{5/2}$ mol Np and $\Delta/k_B=85$ K (see solid line).

The 5*f*-electron entropy $S_{5f}(T)$ for $Np_2PdGa_3$ has been calculated by integrating $C_{5f}(T)/T$ up to 150 K and is depicted in Fig. 4(b). The magnetic entropy increases with increasing temperature to reach a value of 0.4Rln2 at $T_C$. The reduction in the magnetic entropy compared to that expected for doublet ground state (Rln2) is presumably due to the Kondo effect. A large contribution to the 5*f*-electron entropy, obviously originates from the CEF splitting.

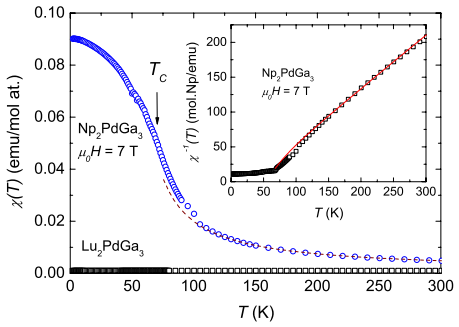


FIG. 5. (Color online) The magnetic susceptibility of $Lu_2PdGa_3$ and $Np_2PdGa_3$ in a field of 7 T as a function of temperature. The dashed line is a MCW fit. The inset shows $\chi^{-1}(T)$ vs $T$ and the solid line is a fit based on the CEF model for data between $T_C$ and 300 K.

### C. Magnetic properties

The magnetic susceptibility $[\chi(T)=M(T)/\mu_0 H]$ of $Lu_2PdGa_3$ and $Np_2PdGa_3$ in a field of 7 T is shown in Fig. 5. As can be seen, the susceptibility of the $Lu_2PdGa_3$ compound is very small and above 100 K remains weakly temperature dependent with $\chi_0=3.3\times10^{-5}$ emu/mol Lu at room temperature. On the other hand, $Np_2PdGa_3$ behaves as a local moment magnet, for which the data can be described by a modified Curie-Weiss (MCW) law: $\chi(T)=N_A\mu_{eff}^2/[3k_B(T-\Theta_p)]+\chi_0$. The theoretical data are shown as dashed line. Above 120 K, the fit of the data yielded a paramagnetic Curie temperature $\Theta_p=46(1)$ K, an effective magnetic moment $\mu_{eff}=2.89(5)$ $\mu_B$/Np and a temperature-independent susceptibility $\chi_0=0.7(1)\times10^{-3}$ emu/mol Np. A large $\Theta_p$-value indicates dominant ferromagnetic exchange interaction in $Np_2PdGa_3$. The observed $\mu_{eff}$ value agrees fairly well with the theoretical value of 2.75 $\mu_B$/Np, expected for the electronic configuration $5f^4$ in the intermediate Russell-Saunders coupling. This may imply that the magnetic moments of Np ions are well localized in $Np_2PdGa_3$. Small $\chi_0$ value of $Np_2PdGa_3$ and $Lu_2PdGa_3$ account for the Pauli-type paramagnetic contribution.

Consistently with the specific-heat data, the susceptibility of $Np_2PdGa_3$ may be analyzed on the basis of a CEF model but exchange effect should be included according to

$$\frac{1}{\chi(T)} = \frac{1}{\chi_{\mathrm{CEF}}(T)+\chi_0} - \lambda, \quad (11)$$

where $\lambda$ is the molecular field constant. We considered the effect of the magnetocrystalline anisotropy in a standard manner, i.e., assuming the average value of the susceptibility as the sum of $\chi_{\mathrm{CEF}}=1/3\chi_{\parallel}+2/3\chi_{\perp}$. The result of fittings of the experimental data suggested that the magnetocrystalline anisotropy of $Np_2PdGa_3$ is very strong, and the measured susceptibility corresponds well to the longitudinal susceptibility, $\chi_{\parallel}$ along the $c$ axis in the hexagonal unit cell. Among six possibilities, a $\Gamma_5^2-\Gamma_6-\Gamma_5^1$ scheme seems to be suitable

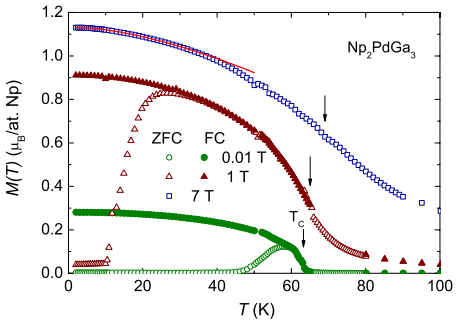


FIG. 6. (Color online) The low-temperature magnetization of $Np_2PdGa_3$ collected at 0.01, 1 T and 7 T in ZFC and FC modes. The solid line is a fit by spin-wave formula Eq. (13).

for the description of the magnetic susceptibility of $Np_2PdGa_3$. The $\chi_{CEF}$ of such splitting is given

$$\chi_{CEF}(T) = \frac{N_A\mu_B^2}{2+2e^{(-\Delta_1/k_BT)}+e^{(-\Delta_2/k_BT)}} \times \left\{ \left[ \frac{|\langle\Gamma_5^2|J_z|\Gamma_5^2\rangle|^2}{k_BT} + 2\frac{|\langle\Gamma_5^2|J_z|\Gamma_6\rangle|^2}{\Delta_1} + \frac{|\langle\Gamma_5^2|J_z|\Gamma_5^1\rangle|^2}{\Delta_2} \right] + \left[ \frac{|\langle\Gamma_6|J_z|\Gamma_6\rangle|^2}{k_BT} - 2\frac{|\langle\Gamma_6|J_z|\Gamma_5^2\rangle|^2}{\Delta_1} + 2\frac{|\langle\Gamma_6|J_z|\Gamma_5^1\rangle|^2}{\Delta_{21}} \right] e^{(-\Delta_1/k_BT)} + \left[ \frac{|\langle\Gamma_5^1|J_z|\Gamma_5^1\rangle|^2}{k_BT} - 2\frac{|\langle\Gamma_5^1|J_z|\Gamma_6\rangle|^2}{\Delta_{21}} - 2\frac{|\langle\Gamma_5^1|J_z|\Gamma_5^2\rangle|^2}{\Delta_2} \right] e^{(-\Delta_2/k_BT)} \right\}. \quad (12)$$

Taking $\Delta_1/k_B=60$ K, $\Delta_2/k_B=180$ K, and $\Delta_{21}/k_B=(\Delta_2-\Delta_1)/k_B$ from the specific-heat fitting, we have fitted the magnetic data for $T>120$ K using Eq. (11). The result of the fit of the data between $T_C$ and 300 K is shown as solid line in the inset of Fig. 5 with $\chi_0=0.1(0.02)\times10^{-3}$ emu/mol Np and $\lambda=14$ mol Np/emu.

The deviation of $\chi(T)$ from the CEF behavior for $T<120$ K could be attributed to ferromagnetic correlations between the Np ions. In fact, $Np_2PdGa_3$ undergoes a ferromagnetic transition at $T_C=62.5$ K, evidenced by a rapid rise in $\chi(T)$ curves. For $Np_2PdGa_3$ the Curie temperature determined as an inflection point of the $\chi(T)$ vs $T$ curve measured at a low field of 0.01 T agrees well with that from the specific-heat measurements. Low-temperature magnetization data for selected magnetic fields are shown in Fig. 6. Below 7 T, $M(T)$ curves reveal a broad maximum below $T_C$, consistent with the development of a ferromagnetic order influenced by a narrow domain wall or strong magnetocrystalline anisotropy. Obviously, the ZFC- and FC-magnetization curves do exhibit an irreversible effect in low magnetic fields. Temperature, where the onset of the irreversible effect appears, shifts down to low temperatures with increasing fields. This can be explained that in order to achieve a reversible magnetization, a large enough magnetic field to overcome the domain and magnetocrystalline anisotropy is required. Except for the domain and magnetocrystalline anisotropy which favor irreversible magnetization, one cannot exclude the possibility of canted ferromagnetic structure causing a big difference in ZFC and FC curves.

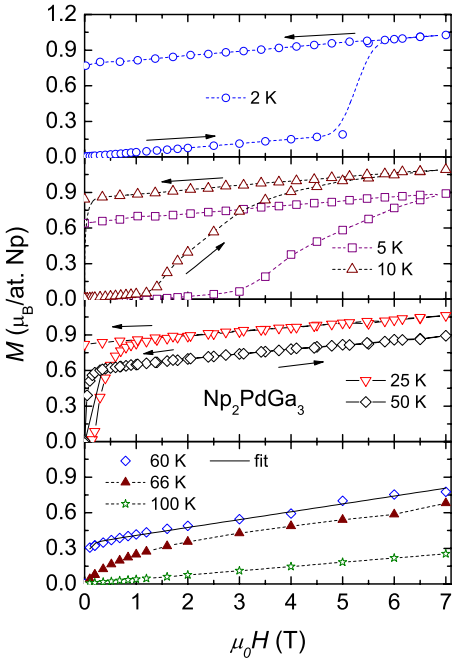


FIG. 7. (Color online) Magnetization of $Np_2PdGa_3$ vs magnetic fields at selected temperatures. The dashed lines are guide for the eyes. The arrow indicate the increasing and decreasing field sweep. The solid line at 60 K data is a fit (see text).

At temperatures low enough below $T_C$ the magnons occurring in anisotropic compound contribute to the magnetization as

$$\frac{M(0)-M(T)}{M(0)} = BT^{3/2}\, exp(-\Delta/k_BT) + \cdots \quad (13)$$

The coefficient $B$ is related to the spin-wave stiffness constant $D$ via

$$B = 2.612\frac{g\mu_B}{M(0)}\left(\frac{k_B}{4\pi D}\right)^{3/2}. \quad (14)$$

A fit of the experimental data of $Np_2PdGa_3$ at 7 T for the temperature range 2–30 K to Eq. (13) yielded $M(0)=1.13(5)$ $\mu_B$, $B=6(0.3)\times10^{-4}$ $K^{-3/2}$, and $\Delta/k_B=7.4(4)$ K. Taking $g=0.6$ for $Np^{3+}$ and $V=60.59$ $Å^3$/Np, we have estimated the value of the spin-wave stiffness coefficient $D$ to be 18.5 meV $Å^2$. The difference in the $\Delta$ values evaluated from the magnetization and specific-heat data suggests a large influence of magnetic fields on the magnetocrystalline anisotropy gap.

Figure 7 shows the field dependence of the magnetization of $Np_2PdGa_3$ at several selected temperatures. The data were collected after zero-field cooling. At 2 K and 7 T, $M$ does not saturate. The steplike magnetization at a critical field $\mu_0H_{cr}$ in the increasing field sweep and quasilinear field dependence of $M(H)$ curves for fields above $\mu_0H_{cr}$ point to a strong magnetocrystalline anisotropy. At 2 K, $\mu_0H_{cr}$ amounts

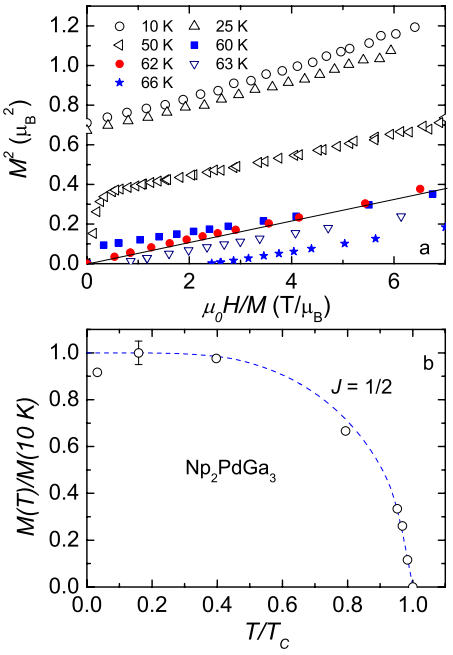


FIG. 8. (Color online) (a) Isotherms of $M^2$ vs $H/M$. (b) The temperature dependence of the spontaneous magnetization with Brillouin function for $J=1/2$.

to about 5 T and decreases with increasing temperature. For data collected with decreasing field sweep, the description by the relation[32]

$$M(H,T) = M_s(T) + a(T)/H + b(T)/H^2 \tag{15}$$

is well satisfied. In the Eq. (15), $M_s$ is the saturation magnetization and the terms $a/H$ and $b/H^2$ are relevant to the local and magnetocrystalline anisotropy, respectively. As a representative example, we show a fit for the data at 60 K in the bottom panel of Fig. 7. It is observed that the $M(H)$ curves have a spontaneous magnetization till $T=62$ K, and just above this temperature the $M(H)$ curves are not linear, expressing short-range magnetic interactions and/or magnetocrystalline anisotropy effect in the paramagnetic state. One notices that the $M_s$ value deduced from Eq. (15) for the data at 2 K is only 0.78 $\mu_B$/Np. The maximal value of ordered moment of $Np^{3+}$ is $gJ\mu_B=2.4$ $\mu_B$, thus there is moment loss by a factor 3. However, if taking into account only a doublet ground state, one compares the experimental value to that expected for $\Gamma_5^2$ (1.2 $\mu_B$). In this case, the moment loss shows a reasonable factor of 0.25. From the specific-heat and resistivity measurements, the reduction in the moment is caused by screening of the localized magnetic moment by the conduction electrons in the presence of Kondo effect.

Figure 8 a shows the Arrott plot for $Np_2PdGa_3$. For $T<50$ K, the spontaneous magnetization values were obtained from the decreasing field sweep data. We observe a positive slope of the $M^2$ vs $H/M$ plot and therefore, we may analyze the data assuming the paramagnetic-ferromagnetic transition to be of second order in this compound. According to the mean-field theory, near $T_C$, $M^2$ vs $H/M$ at various temperatures should show a series of parallel lines and at $T_C$, $M^2$ should pass through the origin.[33] In the case of

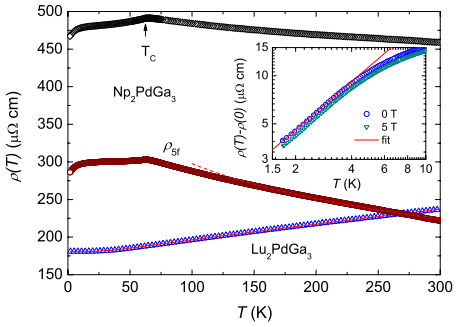


FIG. 9. (Color online) Temperature dependence of the electrical resistivity of $Lu_2PdGa_3$ and $Np_2PdGa_3$. The solid line is a fit to the phonon contributions. 5*f*- electron resistivity is fitted with a ln $T$ dependence for $T>150$ K. The inset shows low-temperature resistivity data.

$Np_2PdGa_3$ $T_C$ is found to be 62.5(5) K. The Arrott plot technique was proposed to distinguish pure ferromagnets from disordered ones.[34] Due to the presence of disorder the slope of $M^2$ vs $H/M$ at low fields should be reduced compared to those in pure ferromagnets but at high fields the $M^2$ vs $H/M$ curves blend upwards. In $Np_2PdGa_3$ a little curvature of $M^2$ vs $H/M$ curve can be recognized at temperatures below 25 K. If assuming that the extrapolated values from the high-field regimes are the spontaneous magnetization without atomic disorder, then $M_s$ at 10 K would attain a value 0.88 $\mu_B$/Np. This value does not differ significantly from the low-field extrapolated value 0.85 $\mu_B$/Np, meaning that the atomic disorder weakly influences on magnetic Np moments. In Fig. 8(b) the reduced spontaneous magnetization as a function of the reduced temperature is plotted for $Np_2PdGa_3$. The validity of the Brillouin function type description is tested for $J=1/2$. A similar behavior was observed for the ordered magnetic moment of ferromagnetic Kondo compound $NpNiSi_2$ determined by the magnetic hyperfine field, suggesting a doublet ground state.[11]

### D. Electrical transport properties

The temperature dependence of the electrical resistivity of $Lu_2PdGa_3$ and $Np_2PdGa_3$ is shown in Fig. 9. The overall temperature $\rho(T)$ dependence of $Lu_2PdGa_3$ is of metallic characteristics. Since any atom involved in $Lu_2PdGa_3$ does not carry local magnetic moment, one expects the resistivity to be governed by scattering of conduction electrons from defects and phonon excitations only. The latter contribution arises from the scattering of electrons with acoustic and optical phonons.

Accordingly, the resistivity of $Lu_2PdGa_3$ can be described using the relation

$$\rho(T) = \rho_0 + df\left(\frac{\Theta_D}{T}\right) + ef\left(\frac{\Theta_E}{T}\right), \tag{16}$$

where $\rho_0$ is the residual resistivity and $d$, and $e$ are numerical constants. The functions $f(\frac{\Theta_D}{T})$ and $f(\frac{\Theta_E}{T})$ are

$$f\left(\frac{\Theta_D}{T}\right) = \frac{1}{\Theta_D}\left(\frac{T}{\Theta_D}\right)^5 \int_0^{\Theta_D/T} \frac{x^5 dx}{(e^x-1)(1-e^{-x})},$$

$$f\left(\frac{\Theta_E}{T}\right) = \frac{\Theta_E}{T}\frac{1}{(e^x-1)(1-e^{-x})}.$$

Keeping $\Theta_D = 315$ K and $\Theta_E = 113$ K obtained from the specific-heat measurement, a fit of the data yielded $\rho_0 = 181(2)$ $\mu\Omega$ cm, $d = 0.10(1)$ $\mu\Omega$ cm K, and $e = 11(1)$ $\mu\Omega$ cm. One may add that including the electron-electron scattering term $\rho_{el-el} \propto AT^2$, a value of $A \sim 10^{-6}$ $\mu\Omega$ cm K$^{-2}$ is obtained. This value is very small, suggesting that the electron-electron scattering is a negligible scattering mechanism in $Lu_2PdGa_3$.

The temperature dependence of $\rho(T)$ of $Np_2PdGa_3$ has an anomaly at $T_C$, corroborating the magnetic phase transition found in specific heat and magnetization. The $5f$-electron contribution to the total resistivity is assumed to be the difference of the measured resistivity of $Np_2PdGa_3$ and $Lu_2PdGa_3$, $\rho_{5f} = \rho_{Np_2PdGa_3} - \rho_{Lu_2PdGa_3}$. Apparently, $\rho_{5f}$ of $Np_2PdGa_3$ is relatively large as it is considered as that of an ordinary metallic ferromagnet. To account for such high resistivity, one considers several factors, for instance atomic disorder, spin disorder and Kondo effect, which basically enlarge electrical resistivity. Of course, possible microcracks and grain boundary scattering cannot be excluded. In a disordered atomic system, large resistivity is caused by inelastic electron-electron collisions. To this mechanism, $1/\rho(T) \sim T$ at low temperatures and $1/\rho(T) \sim \sqrt{T}$ dependence at high temperatures is usually ascribed.[35] For the case of $Np_2PdGa_3$, the crystallographic disorder seems to not manifest $1/\rho(T) \sim \sqrt{T}$ characteristics.

The spin-disorder resistivity due to the interaction between the conduction electrons and spins of magnetic ions in the paramagnetic state is given by de Gennes,[36] $\rho_{sd} = \frac{3\pi N m^*}{2\hbar^2 e^2 E_F} J_{ex}^2 (g-1)^2 J(J+1)$ where $m^*$ is the effective mass, $E_F$ the Fermi energy $N$ the number of atoms per unit volume and $J_{ex}$ the exchange coupling constant. $Np_2PdGa_3$ exhibiting a large $m^*$ value (see below), enormous $J_{ex}$ (as it is proportional to $T_C$) and a high $J$ (=4), should have a large $\rho_{sd}$. The presence of Kondo effect in the studied sample is evidenced by the negative $d\rho_{5f}/dT$ and $\ln T$-dependence for $T > 150$ K (see dashed line in Fig. 9). Moreover, in the framework of the underscreened Kondo model, the resistivity of ferromagnetic Kondo lattices with hybridization gap might display large values accordingly to predicted semimetallic properties.[10]

Below $T_C$, $\rho(T)$ decreases due to a reduction in spin disorder resistivity. However, around 20 K there appears a shoulder similar to the behavior of Kondo scattering from magnetic ions in their CEF ground state. Interestingly, the resistivity of $Np_2PdGa_3$ at low temperatures does show a linear dependence (see inset of Fig. 9), which persists in fields up to 5 T.

Magnetic field weakly influences the electrical resistivity of $Np_2PdGa_3$. At 2 K and 9 T, magnetoresistance $MR$ defined as $[\rho(B,T) - \rho(0,T)]/\rho(0,T)$ is negative and reaches only about $-1\%$. $MR$ becomes positive at $T > T_C$, which originates from the cyclotron motion of conduction electrons. It is worth pointing out that there is a steplike change in the field dependence of $MR$ around 6 T (see inset of Fig. 10). This

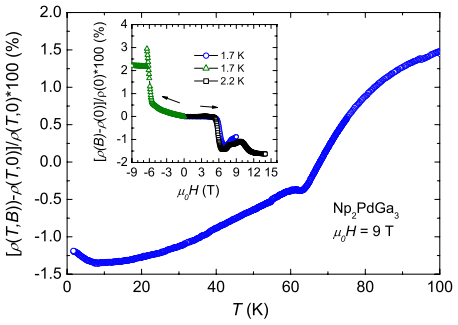


FIG. 10. (Color online) Temperature dependence of the magnetoresistance of $Np_2PdGa_3$ measured at 9 T. The inset shows the field dependence of the magnetoresistance at 1.7 and 2 K.

anomaly coincides with the observed jump in the magnetization at critical field $\mu_0 H_{cr}$. In order to clarify the reason of the anomaly further investigations, notably neutron diffraction or $^{237}$Np-Mössbauer spectroscopy experiments, are needed.

The temperature dependence of the Hall coefficient measured in selected magnetic fields 1, 3, 5, and 9 T is shown in Fig. 11, and the field dependence of the resistivity from transverse contacts at several temperatures is shown in Figs. 12(a)–12(e). A comparison of isotherms and isofield of the Hall effect and magnetization reveals that the temperature and field dependencies of these quantities have similar shape. This observation indicates that a large contribution to $R_H(H)$ results from the magnetization. In order to describe the $R_H(T)$ we used conventional expression for a ferromagnetic metal.

$$R_H = R_0 + R_s M/\mu_0 H. \tag{17}$$

In this equation, the normal Hall effect ($R_0$) is due to Lorentz force on conduction electrons and the anomalous Hall coef-

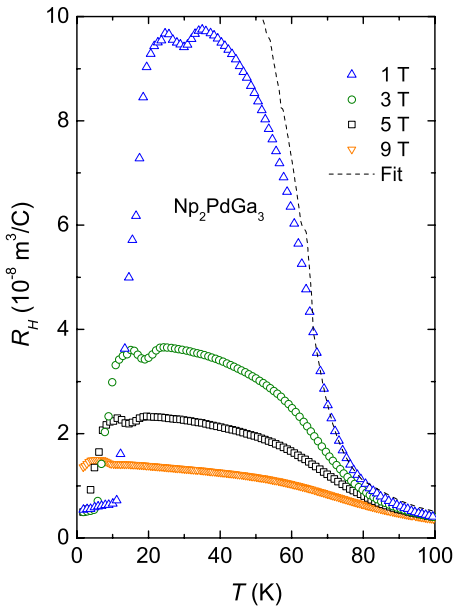


FIG. 11. (Color online) Temperature dependence of the Hall coefficient of $Np_2PdGa_3$ measured at several selected fields up to 9 T. Dashed line is a fit for the data collected at 1 T.

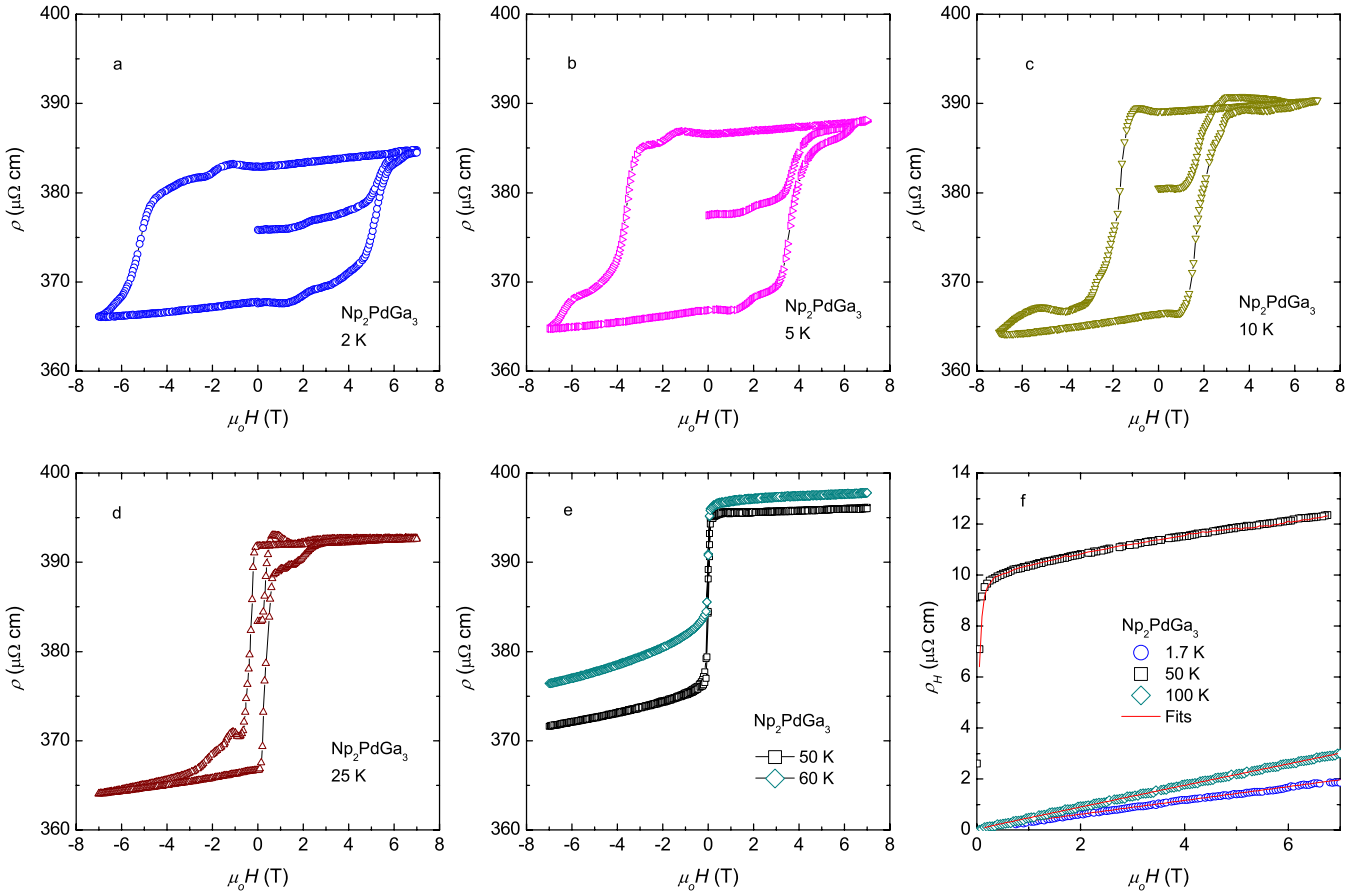


FIG. 12. (Color online) [(a–e)] The field dependence of the resistivity from the transverse contacts. (f) Field dependence of the Hall resistivity at 1.7, 50, and 100 K with respective fits to Eq. (17).

ficient ($R_s$) denotes asymmetric scattering of skew and jump side on magnetic ions.[37,38] As an example, we show in Fig. 11 the result of a fit of data for the paramagnetic state at $\mu_0 H = 1$ T. The dashed line with $R_0 \sim = -1.45 \times 10^{-9}$ m$^3$/C and $R_s \sim 9.24 \times 10^{-8}$ m$^3$/C reproduces well the experimental data for $T > 65$ K. We have analyzed isotherms according to Eq. (17). Representative fits are illustrated for $T = 1.7$, 50, and 100 K [see Fig. 12(f)]. A fit of the data at 100 K to Eq. (17) yielded $R_0 = -1.45 \times 10^{-9}$ m$^3$/C and $R_s = 9.17 \times 10^{-8}$ m$^3$/C. In the one-band model, $R_0$ corresponds to a carrier concentration $n_e = 4.3 \times 10^{27}$ m$^{-3}$ or 0.26 carrier/f.u. For the 1.7 K data we inferred $R_0 = 2.18 \times 10^{-9}$ m$^3$/C and $R_s = 16 \times 10^{-8}$ m$^3$/C. The low-temperature $R_0$ corresponds $2.87 \times 10^{27}$ m$^{-3}$ or 0.17 carrier/f.u. Combining the carrier concentration at 1.7 K with the Sommerfeld coefficient of 120 mJ/K$^2$ mol Np. one estimates an electron effective mass $m^* = 144\ m_0$. Such a large value $m^*$ is reminiscent of those of heavy-fermion materials. The results of fits for all measured temperatures are presented in Fig. 13. As can bee seen, both $R_0$ and $R_s$ show an extremum near $T_C$. The magnitude of $R_s$ is greater than that of $R_0$, implying that $R_H$ is dominated by $R_s$. The negative sign of $R_0$ is found to be unchanged down to about 40 K, which is indicative of electron-type charge carriers. The change in the sign of $R_0$ to positive suggests that both holelike and electronlike carriers coexist in this materials.

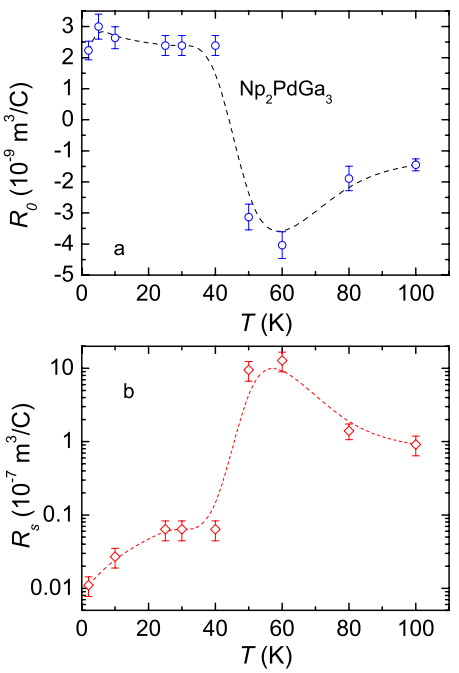


FIG. 13. (Color online) Temperature dependence of the $R_0$ and $R_s$ deduced from fits of the experimental data to Eq. (17).

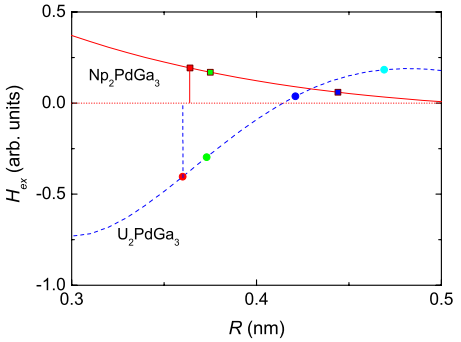


FIG. 14. (Color online) The RKKY exchange energy $H_{ex}$ as a function of distance $R_{i,j}$. The exchange between nearest, next-nearest magnetic atoms and so on are indicated by circles and squares for U and Np, respectively. The vertical lines denote the magnitude of the exchange energy.

## IV. DISCUSSION

Our experimental data point out significant difference in the physical properties between two isostructural actinoid compounds $Np_2PdGa_3$ and $U_2PdGa_3$. We recall that the latter compound behaves as an itinerant electron antiferromagnet with $T_N \sim 30$ K. The Kondo effect and randomness coexist with short-range antiferromagnetism. On the other hand, $Np_2PdGa_3$ is a local moment ferromagnet. The Kondo effect interplays with CEF splitting. In the following we try to explain the change in the magnetic ordering, assuming the existence of RKKY long-range exchange in the $An_2PdGa_3$ compounds.

The fact that a change occurs in both the type of magnetic orderings and the magnitude of ordering temperatures, first of all, reflects an oscillatory character of the exchange interactions. For $U_2PdGa_3$ and $Np_2PdGa_3$ the *An-An* distances ($\sim$0.362 nm) are larger than the Hill value ($\approx$0.35 nm), limiting direct interactions. Instead, the *An-L* distances ($\sim$0.17 nm) are relatively short, allowing a strong hybridization of 5*f* and conduction electron states. These facts imply that the indirect exchange mediated via the conduction electrons favors a long-range order, and direct exchange must be a minor mechanism in $An_2PdGa_3$. In the RKKY formalism, the exchange Hamiltonian $H_{ex} \propto -J_{ex}^2 \Sigma_{i,j} F(R_{i,j}) S_i S_j$ describes the oscillatory character of interactions between local spin $S_i$ and $S_j$ separated with the interionic distance $R_{ij}$. The function $F(R_{i,j})$ is defined as: $F(R_{i,j}) = [2k_F R \cos(2k_F R) - \sin(2k_F R)]/R^4$, where $k_F$ is the Fermi wave vector. Calculating $k_F = (3\pi^2 n_e)^{1/3}$ from the Hall carrier concentration $n_e$ data ($k_F = 0.93$ Å$^{-1}$ for $U_2PdGa_3$ an $k_F = 0.44$ Å$^{-1}$ for $Np_2PdGa_3$) and assuming $J_{ex} \propto M_{ord}$ ($M_{ord} = 0.4$ $\mu_B/U$ and $M_{ord} = 0.8$ $\mu_B$/Np) we plot in Fig. 14 the RKKY exchange energy $H_{ex}$ as a function of distance $R_{i,j}$. On the basis of Fig. 14 the changes in type of magnetic ordering and magnitude of the phase transition temperatures can be qualitatively understood. In $U_2PdGa_3$ the interactions between both nearest and N-nearest magnetic ions are antiferromagnetic whereas these interactions in $Np_2PdGa_3$ are ferromagnetic.

From the crystallographic point of view, the degree of atomic disorder in $U_2PdGa_3$ and $Np_2PdGa_3$ is the same. However, the 5*f* electron in $Np_2PdGa_3$ are much more localized than in $U_2PdGa_3$. The replacement of short-range in U based by long-range order in Np-based compound has a source also in RKKY interactions. One of the possible mechanism for short-range ordering is the competition of ferromagnetic and antiferromagnetic interactions. This situation could happen in $U_2PdGa_3$ when the average amplitude of RKKY of interactions between nearest, N- nearest (of antiferromagnetic character) and NN-nearest, NNN-nearest (of ferromagnetic character) magnetic uranium ions is close to zero (see Fig. 14). The long-range ferromagnetic ordering observed in $Np_2PdGa_3$ accords with positive values of $H_{ex}$.

Finally, we attempt to understand the enhancement in the effective mass of carriers in ferromagnetic, localized electron $Np_2PdGa_3$ compound. The analysis of specific-heat and electron transport properties shown above leads to the assertion that the Kondo effect is the main mechanism responsible for large Sommerfeld ratio and small Fermi momentum, corresponding to a large effective mass of charge carriers in $Np_2PdGa_3$. Recently, Perkins *et al.*[10] developed an UKL model, which assumes a periodic lattice of magnetic atoms with $S=1$ interacting with a spin density of conduction electrons via an on-site antiferromagnetic Kondo coupling. According to the authors, there is presence of two *f* levels; one nonhybridized and one hybridized level. The nonhybridized level with energy $E_{0\sigma}$ lies inside the hybridization gap $\Gamma_\sigma$ for the spin-up band due to the Kondo effect and inside the conduction band for the spin-down band. A mass enhancement is explained by $m^*/m = \frac{\alpha_\sigma^2}{(E_{0,\sigma}-\mu-\Delta_\sigma)^2}$, where $\alpha \propto \Gamma_\sigma$, $\mu$ is a chemical potential and $\Delta_\sigma$ is an energy shift for conduction electron band. The UKL model, therefore, can provide an explanation for the enhanced effective mass of carriers and semimetallic-like properties of $Np_2PdGa_3$.

## V. CONCLUSIONS

In conclusion, we have synthesized two intermetallics $Lu_2PdGa_3$ and $Np_2PdGa_3$ crystallizing in an orthorhombic $CeCu_2$-type structure (space group *Imma*). The electronic properties of these compounds were characterized by magnetization, electrical resistivity, and specific-heat measurements. The metallic, nonmagnetic properties of $Lu_2PdGa_3$, used as a phonon reference for $Np_2PdGa_3$. The specific heat and electrical resistivity of $Lu_2PdGa_3$ can be well described by the Debye and Einstein functions. For $Lu_2PdGa_3$ the Sommerfeld ratio of $\sim$2.3 mJ/K$^2$ mol Lu, and temperature-independent paramagnetism of $\sim 10^{-5}$ emu/mol Lu were observed. In the case of $Np_2PdGa_3$, it was established that this compound orders ferromagnetically below 62.5(5) K. The analysis of specific heat and magnetic susceptibility consistently suggests a CEF splitting with doublet-doublet-doublet scheme and splitting energies $\Delta_{CEF} \sim 60$ K and 180 K. The enhanced Sommerfeld ratio at low temperature and ln *T* dependence of the resistivity can be interpreted by the Kondo effect with $T_K \sim 35$ K. The Hall coefficient exhibits a behavior for localized moment ferromagnets with low-carrier concentration (0.17 carrier/f.u) or with enhanced effective mass ($\sim$144 $m_0$). The presented data are consistent with the UKL model recently developed by Perkins *et al.* Hence, we

argue that $Np_2PdGa_3$ is the Np-based ferromagnetic Kondo lattice with $T_K < T_{RKKY} \approx \Delta_{CEF}$.

## ACKNOWLEDGMENTS

The authors thank R. Caciuffo for critical reading and valuable discussions. We acknowledge the financial support to users provided by the European Commission within the "Actinide User Laboratorium" program at ITU (Contract No. RITA 2006-026176). We are grateful to D. Bouëxière and S. Uhle for their technical assistance. The high purity Np metal required for the fabrication of the compound was made available through a loan agreement between Lawrence Livermore National Laboratory and ITU, in the frame of a collaboration involving LLNL, Los Alamos National Laboratory, and the U.S. Department of Energy.

[1] D. Kaczorowski and H. Noel, J. Phys.: Condens. Matter **5**, 9185 (1993).
[2] B. Chevalier, R. Pottgen, B. Darriet, P. Gravereau, and J. Etourneau, J. Alloys Compd. **233**, 150 (1996).
[3] V. H. Tran, J. Phys.: Condens. Matter **8**, 6267 (1996).
[4] D. X. Li, Y. Shiokawa, Y. Homma, A. Uesawa, A. Dönni, T. Suzuki, Y. Haga, E. Yamamoto, T. Honma, and Y. Onuki, Phys. Rev. B **57**, 7434 (1998).
[5] D. X. Li, A. Donni, Y. Kimura, Y. Shiokawa, Y. Homma, Y. Haga, E. Yamamoto, T. Honma, and Y. Onuki, J. Phys.: Condens. Matter **11**, 8263 (1999).
[6] D. X. Li, S. Nimori, Y. Shiokawa, Y. Haga, E. Yamamoto, and Y. Onuki, Phys. Rev. B **68**, 172405 (2003).
[7] V. H. Tran, F. Steglich, and G. André, Phys. Rev. B **65**, 134401 (2002).
[8] K. A. Gschneidner, Jr., J. Tang, S. K. Dhar, and A. Goldman, Physica B **163**, 507 (1990).
[9] V. H. Tran, Mater. Sci. (Poland) **26**, 1069 (2008).
[10] N. B. Perkins, M. D. Núñez-Regueiro, B. Coqblin, and J. R. Iglesias, Phys. Rev. B **76**, 125101 (2007).
[11] E. Colineau, F. Wastin, J. P. Sanchez, and J. Rebizant, J. Phys.: Condens. Matter **20**, 075207 (2008).
[12] R. Caciuffo, J. A. Paixão, C. Detlefs, M. J. Longfield, P. Santini, N. Bernhoeft, J. Rebizant, and G. H. Lander, J. Phys.: Condens. Matter **15**, S2287 (2003).
[13] G. H. Lander, L. Heaton, M. H. Mueller, and K. D. Anderson, J. Phys. Chem. Solids **30**, 733 (1969).
[14] Y. N. Grin, O. M. Sichevich, and O. R. Myakush, Sov. Phys. Crystallogr. **36**, 503 (1991).
[15] T. Roisnel and J. Rodriguez-Carvjal, *Materials Science Forum*, Proceedings of the Seventh European Powder Diffraction Conference, edited by R. Delhez and E. J. Mittenmeijer, Barcelona, 20–23 May 2000, pp. 118–123.
[16] L. A. Boatner and M. M. Abraham, Rep. Prog. Phys. **41**, 87 (1978).
[17] E. S. R. Gopal, *Specific Heats at Low Temperatures* (Plenum, New York, 1996).
[18] B. D. Dunlap and G. H. Lander, Phys. Rev. Lett. **33**, 1046 (1974).
[19] B. D. Dunlap, M. B. Brodsky, G. M. Kalvius, G. K. Shenoy, and D. J. Lam, J. Appl. Phys. **40**, 1495 (1969).
[20] I. Yaar, S. Fredo, J. Gal, W. Potzel, G. M. Kalvius, and F. J. Litterst, Phys. Rev. B **45**, 9765 (1992).
[21] Y. Homma, M. Nakada, A. Nakamura, S. Nasu, D. Aoki, H. Sakai, S. Ikeda, E. Yamamoto, Y. Haga, Y. Onuki, and Y. Shiokawa, Hyperfine Interact. **168**, 1175 (2006).
[22] E. Colineau, P. Javorský, P. Boulet, F. Wastin, J. C. Griveau, J. Rebizant, J. P. Sanchez, and G. R. Stewart, Phys. Rev. B **69**, 184411 (2004).
[23] E. Colineau, F. Wastin, P. Boulet, P. Javorský, J. Rebizant, and J. P. Sanchez, J. Alloys Compd. **386**, 57 (2005).
[24] K. D. Schotte and U. Schotte, Phys. Lett. A **55**, 38 (1975).
[25] C. D. Bredl, F. Steglich, and K. D. Schotte, Z. Phys. B **29**, 327 (1978).
[26] V. H. Tran, R. Troć, Z. Bukowski, D. Badurski, and C. Sułkowski, Phys. Rev. B **71**, 094428 (2005).
[27] H. v. Löhneysen, R. van den Berg, J. Wosnitza, G. V. Lecomte, U. Krey, and W. Zinn, *Magnons in spin-glasses in zero-field and in high magnetic fields: Experiments and theory*, Lecture Notes in Physics Vol. 275 (Springer, Berlin/Heidelberg, 1987), pp. 51–59.
[28] J. G. Sereni, *Encyclopedia of Materials, Science Technology*, edited by K. H. Buschow and E. Gratz (Elsevier Science, New York, 2001), Vol. 5, pp. 4986–4994.
[29] B. Coqblin and R. J. Schrieffer, Phys. Rev. **185**, 847 (1969).
[30] V. T. Rajan, Phys. Rev. Lett. **51**, 308 (1983).
[31] J. A. Blanco, M. de Podesta, J. I. Espeso, J. C. Gómez Sal, C. Lester, K. A. McEwen, N. Patrikios, and J. Rodríguez Fernández, Phys. Rev. B **49**, 15126 (1994).
[32] S. Chikazumi, *Physics of Ferromagnetism* (Oxford University Press, New York, 1964), p. 274.
[33] A. Arrott, Phys. Rev. **108**, 1394 (1957).
[34] I. Yeung, R. M. Roshko, and G. Williams, Phys. Rev. B **34**, 3456 (1986).
[35] P. A. Lee and T. V. Ramakrishnan, Rev. Mod. Phys. **57**, 287 (1985).
[36] P. G. de Gennes, J. Phys. Radium **23**, 510 (1962).
[37] J. Smit, Physica (Amsterdam) **24**, 39 (1958).
[38] L. Berger, Phys. Rev. B **2**, 4559 (1970).